Chemistry Publications and Other Works

Chemistry

1-1-2006

Interaction-induced dipole moment of the Ar–H$_2$ dimer: dependence on the H$_2$ bond length

Robert J. Hinde

University of Tennessee - Knoxville, rhinde@utk.edu

Follow this and additional works at: http://trace.tennessee.edu/utk_chempubs

Part of the Atomic, Molecular and Optical Physics Commons, Biological and Chemical Physics Commons, and the Physical Chemistry Commons

Interaction-induced dipole moment of the Ar–H$_2$ dimer: Dependence on the H$_2$ bond length

Robert J. Hinde[a)]

Department of Chemistry, University of Tennessee, Knoxville, Tennessee 37996-1600

We present *ab initio* calculations of the interaction-induced dipole moment of the Ar–H$_2$ van der Waals dimer. The primary focus of our calculations is on the H$_2$ bond length dependence of the dipole moment, which determines the intensities of both the collision-induced H$_2$ $v=1\leftarrow0$ fundamental band in gaseous Ar–H$_2$ mixtures and the dopant-induced H$_2$ $v=1\leftarrow0$ absorption feature in Ar-doped solid H$_2$ matrices. Our calculations employ large atom-centered basis sets, diffuse bond functions positioned between the two monomers, and a coupled cluster treatment of valence electron correlation; core-valence correlation effects appear to make negligible contributions to the interaction-induced dipole moment for the Ar–H$_2$ configurations considered here. © *2006 American Institute of Physics.* [DOI: 10.1063/1.2173242]

I. INTRODUCTION

Studies of the interaction-induced electrical properties of weakly bound dimers provide us with information about the redistribution of electron density that accompanies dimer formation and thus with insight into the origins of intermolecular forces. This has stimulated a number of *ab initio* investigations of the interaction-induced multipole moments and polarizabilities of weakly bound dimers. From a more practical viewpoint, these interaction-induced electrical properties provide a starting point for computations of collision-induced absorption line shapes and for the analysis of collision-induced light scattering phenomena.

In this paper we present coupled cluster *ab initio* calculations of the interaction-induced dipole moment of the Ar–H$_2$ van der Waals dimer. Meyer and Frommhold[1] have reported *ab initio* calculations of the interaction-induced Ar–H$_2$ dipole moment for geometries in which the H$_2$ fragment is held at its vibrationally averaged $v=0$ bond length. Here, we investigate the dependence of this dipole moment on the H$_2$ bond length and calculate the interaction-induced H$_2$ vibrational transition dipole moment for Ar–H$_2$ dimers.

Our work is motivated by the recent observation of dopant-induced H$_2$ $Q_1(0)$ features in the infrared absorption spectra of H$_2$ solids containing low concentrations of rare gas dopants.[2] We have explained elsewhere[3] that these features arise from symmetry breaking of the solid H$_2$ crystal lattice in the vicinity of the dopant; hence they can be viewed as solid-phase analogs of collision-induced absorption phenomena. The Ar–H$_2$ vibrational transition dipole moments computed here control the intensity of the dopant-induced H$_2$ $Q_1(0)$ absorption feature, and could ultimately be used in theoretical calculations of the line shape of this feature for comparison with experimental observations.

Of course, the transition moments computed here also control the intensities of collision-induced absorption features observed in gaseous Ar–H$_2$ mixtures[4] in the vicinity of the H$_2$ $Q_1(0)$ and $S_1(0)$ transitions. The line shapes of these features can be computed from first principles[5] using the transition moments presented here and an accurate Ar–H$_2$ interaction potential.[6] Comparing the theoretical line shapes of these features with those that have been measured experimentally would therefore help test the accuracy of the present calculations.

II. COMPUTATIONAL METHODS

We compute the interaction-induced dipole moment M for the Ar–H$_2$ dimer as the derivative of the Ar–H$_2$ interaction potential V with respect to the magnitude of an externally applied homogeneous electric field F: $M = -(\partial V / \partial F)_{F=0}$. The interaction potential V is the sum of a frozen-core term V_{FC}, in which only the H$_2$ electrons and the outermost eight Ar electrons are correlated, and a core-valence correction term V_{CV}; we will find, however, that the core-valence term makes a negligible contribution to the interaction-induced dipole moment of the dimer. Both V_{FC} and V_{CV} are computed using Gaussian[7] at the CCSD(T) level of theory[8–10] and employ the standard counterpoise correction.[11]

Our frozen-core calculations employ aug-cc-pVTZ atom-centered basis sets[12,13] that have been extended with an additional atom-centered set of diffuse functions. The added functions consist of one additional primitive Gaussian of each symmetry present in the standard aug-cc-pVTZ basis sets, with an exponent one-third as large as the smallest exponent of that symmetry. Frozen-core CCSD(T) calculations of the individual Ar and H$_2$ monomers using these atom-centered basis sets give electrical properties (Ar and H$_2$ polarizabilities, H$_2$ quadrupole moment) in good agreement with literature values.[14–16] For the Ar–H$_2$ dimer calculations, we place a $(3s3p2d)$ set of bond functions[17] midway between the Ar nucleus and the H$_2$ center of mass to improve the description of dispersion interactions.[18,19]
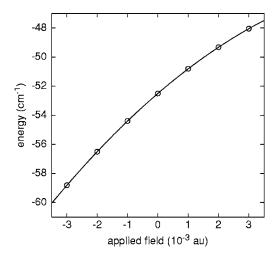
FIG. 1. Dependence of the frozen-core Ar–H_2 interaction energy on F at $R=6.856 \, a_0$, $r=1.401 \, a_0$, and $\gamma=0$. The line is a second-degree polynomial fit to the *ab initio* calculations. In these calculations, the external field is oriented along the z axis.

FIG. 2. Dependence of the frozen-core Ar–H_2 dipole moment on γ at $R=5 \, a_0$ and $r=1.4 \, a_0$. The open circles indicate values of $M_{FC,x}$; the open squares indicate values of $M_{FC,z}$. The lines are fits to truncated Legendre polynomial expansions [Eqs. (1) and (2)] as described in the text.

The core-valence correction term V_{CV} is computed using the aug-cc-pCVTZ basis set[12] for Ar, the aug-cc-pVTZ basis set for H, and the $(3s3p2d)$ set of bond functions. We define V_{CV} as the difference between the interaction energy calculated using this basis set in the frozen-core approximation and the interaction energy calculated using the same basis set when all electrons are correlated.

We describe the configuration of the Ar–H_2 dimer using Jacobi coordinates, in which R is the Ar–H_2 distance, r is the H–H bond length, and γ is the angle between the Ar–H_2 vector and the H–H bond. For specificity, we place the dimer in the (x,z) plane with the Ar atom at the origin and the H_2 center of mass on the positive z axis; when $0 < \gamma < \pi/2$, the H atom which is closer to Ar has a positive x coordinate.

The derivative $(\partial V/\partial F)_{F=0}$ is estimated from a finite-difference analysis of the interaction energies obtained when the dimer is perturbed by external fields of strength $F = \pm 0.001$ a.u. Such an analysis gives accurate dipole moments if the interaction energy can be expressed as a second-degree polynomial in F for small values of F. To test this, we compute the frozen-core interaction energy for the Ar–H_2 dimer at $R=6.856 \, a_0$, $r=1.401 \, a_0$, and $\gamma=0$ as a function of field strength for an external field oriented along the z axis. Our results, shown in Fig. 1, indicate that V_{FC} can be fit by a second-degree polynomial in F, so that the finite-difference analysis employed here should give reliable dipole moments.

The field-free frozen-core Ar–H_2 interaction energy we obtain for this configuration, $V_{FC}=-52.50$ cm^{-1}, is in excellent agreement with the value of -52.56 cm^{-1} obtained from a frozen-core CCSD(T) calculation[20] employing the aug-cc-pV5Z basis set for H and the d-aug-cc-pV5Z basis set for Ar. This demonstrates that bond functions can effectively compensate for inadequacies of atom-centered Gaussian basis sets in computing the binding energy of weakly bound dimers.

The empirical Ar–H_2 potential presented in Ref. 6, which has been adjusted to reproduce a variety of experimental data for the Ar–H_2 dimer, gives an interaction energy of $V=-55.18$ cm^{-1} for this configuration. Although the
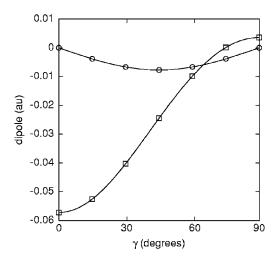
Ar–H_2 binding energy obtained here is slightly smaller than that predicted in Ref. 6, we find that for $r=1.4 \, a_0$ and $5 \, a_0 \leqslant R \leqslant 10 \, a_0$, the frozen-core interaction-induced Ar–H_2 dipole moments at $\gamma=0$ and $\gamma=\pi/2$ change by less than 1% when the extended triple-zeta atom-centered basis sets used are replaced by either larger aug-cc-pVQZ basis sets or smaller aug-cc-pVTZ basis sets. This indicates that the atom-centered basis sets used here are large enough to yield converged interaction-induced dipole moments at the CCSD(T) level, at least when they are combined with a small set of bond functions. (The quadruple-zeta dipole moments are computed from interaction energies obtained using DALTON.[21])

At a fixed Ar–H_2 distance R, the Cartesian components of the interaction-induced dipole moment can be written as[22]

$$M_x = \sum_{k=0}^{\infty} \sum_{j=1}^{\infty} C_{2j,k} P_{2j}^1(\cos \gamma)(r-r_0)^k, \qquad (1)$$

$$M_z = \sum_{k=0}^{\infty} \sum_{j=0}^{\infty} D_{2j,k} P_{2j}(\cos \gamma)(r-r_0)^k, \qquad (2)$$

where P_n is a Legendre polynomial, P_n^m is an associated Legendre polynomial, and r_0 is a reference H_2 bond length which we choose to be $1.4 \, a_0$ here. Figure 2 shows the angular dependence of $M_{FC,x}$ and $M_{FC,z}$ for Ar–H_2 at $R=5 \, a_0$ and $r=1.4 \, a_0$. The *ab initio* results are accurately reproduced by a fit that includes the $j=1$ term in Eq. (1) and the $j=0$ through $j=2$ terms in Eq. (2).

To determine the number of powers of $(r-r_0)$ that must be retained in Eqs. (1) and (2), we calculate $M_{FC,x}$ and $M_{FC,z}$ for Ar–H_2 as functions of r at $R=5 \, a_0$ and three values of γ; our results are shown in panels (a) and (b) of Fig. 3. We see that for r values between $r=0.9 \, a_0$ and $2.1 \, a_0$, truncating these power series expansions at $(r-r_0)^2$ is adequate.

Figure 3(c) shows the core-valence contribution to M_z for Ar–H_2 at $R=5 \, a_0$ and $\gamma=0$; it is also described reasonably well by a second-degree polynomial fit. (The slight scatter in the points reflects the finite precision of the underlying
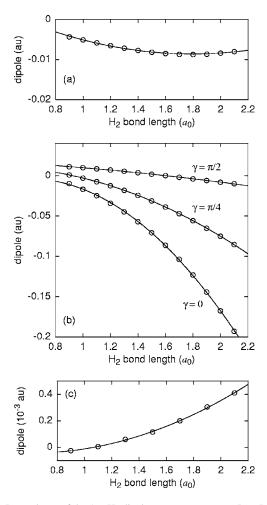
FIG. 3. Dependence of the Ar–H$_2$ dipole moment on r at $R=5$ a_0. Panel (a) shows $M_{FC,x}$ as a function of r at $\gamma=\pi/4$; panel (b) shows $M_{FC,z}$ as a function of r at three γ values; panel (c) shows the core-valence contribution to M_z as a function of r at $\gamma=0$. The solid lines are second-degree polynomial fits to the *ab initio* calculations.
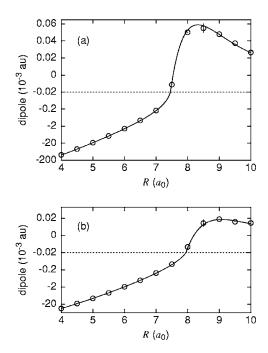

FIG. 4. Dependence on R of (a) the rovibrationally averaged frozen-core Ar–H$_2$ dipole moment $\langle A_{0,1}\rangle_{00}$ and (b) the frozen-core Ar–H$_2$ $Q_1(0)$ transition dipole moment $\langle A_{0,1}\rangle_{01}$. The lines are fits to the data using the parameters listed in Table II. The vertical bars at $R=8.5$ a_0 represent 95% confidence limit intervals; see text for details. Note the change from linear to logarithmic scale in both plots at $\langle A_{0,1}\rangle = -2 \times 10^{-5}$ a.u.

ab initio total energies used to compute the interaction energy V and thus the dipole moment M.) The core-valence correction term is more than two orders of magnitude smaller than the frozen-core dipole moment $M_{FC,z}$ shown in Fig. 3(b). At larger R values, we anticipate that the core-valence correction will be even less important. We therefore dispense with this correction term and report only frozen-core interaction-induced dipole moments here.

III. RESULTS AND DISCUSSION

Figures 2 and 3 show that we can determine the coefficients of the leading terms in Eqs. (1) and (2) for a given R value by computing the Ar–H$_2$ dipole moment at nine configurations, specified by three choices for r and three choices for γ. Here we choose $r=1.1$ a_0, 1.4 a_0, and 1.7 a_0, and $\gamma=0$, $\pi/4$, and $\pi/2$. We calculate the frozen-core Ar–H$_2$ dipole moment at these nine configurations for several R values between 4 a_0 and 10 a_0; the results of these calculations are available through EPAPS.[23]

The Ar–H$_2$ interaction-induced dipole moment gives rise to collision-induced absorption features in gaseous Ar–H$_2$ mixtures.[4,24,25] The line shapes of these collision-induced features can be computed from first principles[1,5,26] if

the Ar–H$_2$ potential surface and dipole moment function are known. For these line shape calculations, it is convenient to express the interaction-induced dipole moment in terms of its spherical tensor components M_ν ($\nu=0,\pm1$), which are related to the Cartesian dipole moments through

$$M_0 = M_z \quad \text{and} \quad M_{\pm1} = \mp (M_x \pm iM_y)/\sqrt{2}. \quad (3)$$

The spherical dipole components M_ν can in turn be expanded in terms of symmetry-adapted functions:[27]

$$M_\nu(\mathbf{r},\mathbf{R}) = \frac{4\pi}{\sqrt{3}}\sum_{\lambda,L} A_{\lambda,L}(r,R)$$
$$\times \sum_\mu \langle \lambda,\mu;L,\nu-\mu|1,\nu\rangle Y_{\lambda,\mu}(\hat{\mathbf{r}})Y_{L,\nu-\mu}(\hat{\mathbf{R}}), \quad (4)$$

where $\langle j_1,m_1;j_2,m_2|J,M\rangle$ is a Clebsch-Gordan coefficient, $\mathbf{R}$ is the vector from the Ar atom to the H$_2$ center of mass, and $\mathbf{r}$ is the vector from one H atom to the other. From our *ab initio* calculations, we can estimate the leading few terms in Eq. (4); the values for the corresponding expansion coefficients $A_{\lambda,L}(r,R)$ are also available via EPAPS.[23] At $r=1.4$ a_0, our $A_{\lambda,L}$ values have magnitudes in qualitative agreement with those computed for $r=1.449$ a_0 in Ref. 1; the sign differences between the two sets of coefficients arise from different choices of the molecule-fixed coordinate system.

At a fixed value of R, we can integrate the expansion coefficients $A_{\lambda,L}(r,R)$ over specific H$_2$ rovibrational wave functions to obtain rovibrationally averaged dipole moments and rotationally averaged transition dipole moments. In Fig. 4, we present the rovibrationally averaged Ar–H$_2$ dipole moment,

TABLE I. H_2 vibrational integrals $\langle v_1=0,j=0|(r-r_0)^n|v_2,j=0\rangle$.

v_2	$n=1$ (a_0)	$n=2$ (a_0^2)
0	0.048 34	0.030 53
1	0.166 39	0.026 74

$$\langle A_{0,1}\rangle_{00} = \langle v=0,j=0|A_{0,1}|v=0,j=0\rangle, \qquad (5)$$

and the $Ar-H_2$ $Q_1(0)$ $v=1\leftarrow 0$ transition dipole moment,

$$\langle A_{0,1}\rangle_{01} = \langle v=0,j=0|A_{0,1}|v=1,j=0\rangle. \qquad (6)$$

These functions were computed using the integrals $\langle v_1=0,j=0|(r-r_0)^n|v_2,j=0\rangle$ summarized in Table I, which were derived from H_2 wave functions obtained from the Kołos-Wolniewicz potential energy curve[15] via the Numerov-Cooley[28] method.

As we noted in our discussion of Fig. 3(c), the interaction-induced dipole moments computed using the finite-field perturbation method employed here suffer from random errors that originate in the finite precision with which the underlying CCSD(T) $Ar-H_2$ interaction energies are computed. Based on the degree of scatter in the points shown in Fig. 3(c), we estimate the magnitudes of these random errors to be 10^{-5} a.u. or less for a given $Ar-H_2$ configuration. If we propagate these random errors forward through the fitting procedure used to extract the expansion parameter $A_{0,1}$ from the computed dipole moments, we obtain the 95% confidence limit intervals for $\langle A_{0,1}\rangle$ shown in Fig. 4.

We have performed similar computations to obtain the rovibrationally averaged quantities $\langle A_{2,3}\rangle_{00}$ and $\langle A_{2,1}\rangle_{00}$ and the transition moments $\langle A_{2,3}\rangle_{01}$ and $\langle A_{2,1}\rangle_{01}$. For line shape calculations, it is convenient to fit these quantities to simple functions of R; we find that an expression of the form

$$D_n/R^n + B\exp(c_1 R + c_2 R^2) \qquad (7)$$

describes $\langle A_{0,1}\rangle$ and $\langle A_{2,3}\rangle$ fairly well, while a similar expression omitting the inverse-power term D_n/R^n provides a good description of the anisotropic overlap term $\langle A_{2,1}\rangle$. The long-range behavior of $\langle A_{2,3}\rangle$ is determined by the Ar polarizability[14] and the H_2 quadrupole moment matrix elements[29] $\langle v=0|Q|v=0\rangle$ and $\langle v=0|Q|v=1\rangle$; this constrains the value of the inverse-power coefficient in the $\langle A_{2,3}\rangle$ fits. The parameters for Eq. (7) are listed in Table II. We emphasize that the D_7 dispersion dipole coefficients given here for the isotropic dipole moments $\langle A_{0,1}\rangle_{00}$ and $\langle A_{0,1}\rangle_{01}$ are *effec-*

tive coefficients that implicitly incorporate contributions from higher-order dispersion dipoles; pure long-range dispersion dipole coefficients of any order can be computed from the imaginary-frequency polarizabilities of the Ar and H_2 monomers.[30]

Our $\langle A_{0,1}\rangle_{00}$ and $\langle A_{2,3}\rangle_{00}$ functions for $Ar-H_2$ are in good agreement with those presented in Ref. 1, where the vibrationally averaged quantities $\langle A_{\lambda,L}\rangle_{00}$ were estimated by performing *ab initio* calculations for $Ar-H_2$ dimers with the H_2 fragment frozen at its $v=0$ vibrationally averaged bond length. This is because the H_2 rovibrational integral $\langle v=0,j=0|(r-r_0)^2|v=0,j=0\rangle$ is relatively small (see Table I) and the coefficients with $k=2$ in Eqs. (1) and (2) therefore make small contributions to the vibrationally averaged moments $\langle A_{\lambda,L}\rangle_{00}$ for $Ar-H_2$ distances $R>5$ a_0.

At large R, the rotationally averaged overlap-induced dipole moment $A_{0,1}$ (computed at a fixed H_2 bond length) arises from long-range dispersion interactions that shift the electron density of the Ar and H_2 monomers into the intermonomer region, creating "local dipoles" associated with each monomer.[31] These local dipoles point along the z axis but are antiparallel to one another; the dipole associated with the H_2 monomer is larger in magnitude, so that the overall $Ar-H_2$ dipole moment has a positive z component. As the monomers approach one another more closely, overlap interactions between the monomers squeeze electron density *out* of the intermonomer region, and the "back" sides of the two monomers acquire excess negative charge. This ultimately reverses the direction of the rotationally averaged dipole moment $A_{0,1}$ at small R values. Inspection of the EPAPS data[23] shows that the reversal happens at larger R values, and is more abrupt, for large values of the H_2 bond length r; this is in accord with a simple model in which Pauli repulsion forces electron density out of the intermonomer region as the two closed-shell monomers approach each other.

The $\langle A_{0,1}\rangle_{00}$ rovibrationally averaged $Ar-H_2$ overlap-induced dipole moment contributes to the far-infrared absorption spectrum of gaseous $Ar-H_2$ mixtures; however, except for frequencies below about 200 cm^{-1}, this contribution is swamped by the far greater contribution made by the $\langle A_{2,3}\rangle_{00}$ function.[1] Unfortunately, measurements of the absorption coefficient of gaseous $Ar-H_2$ mixtures at frequencies below 200 cm^{-1} are rather scarce, so that the gas-phase spectroscopic data currently available are insufficient to provide an experimental test of the overlap-induced $\langle A_{0,1}\rangle_{00}$ function presented here. Experimental measurements of the far-infrared pure translational absorption band in *liquid*

TABLE II. Fitting parameters for Eq. (7), given in a.u.

Component	n	D_n	B	c_1	c_2
$\langle A_{0,1}\rangle_{00}$	7	277.3	−24.992	−1.1125	−0.058 72
$\langle A_{0,1}\rangle_{01}$	7	166.5	−4.667	−0.9642	−0.048 26
$\langle A_{2,3}\rangle_{00}$	4	−9.280	−0.419	−0.6180	−0.063 16
$\langle A_{2,3}\rangle_{01}$	4	−1.687	−0.273	−0.6380	−0.067 22
$\langle A_{2,1}\rangle_{00}$	⋯	⋯	2.843	−0.7582	−0.080 80
$\langle A_{2,1}\rangle_{01}$	⋯	⋯	1.082	−0.7978	−0.069 78

Ar–H_2 mixtures are available and could provide a test for the rovibrationally averaged overlap-induced Ar–H_2 dipole moments computed in this work.[32]

The transition moment functions $\langle A_{\lambda,L} \rangle_{01}$ control the line shapes of the collision-induced absorption features observed in gaseous Ar–H_2 mixtures in the H_2 $v=1 \leftarrow 0$ fundamental band.[4] First-principles calculations of the line shapes of these features, using the transition moments presented here, would test the r dependence of our $A_{\lambda,L}(r,R)$ functions; these calculations are currently underway and will be reported in due course.

ACKNOWLEDGMENTS

[1] W. Meyer and L. Frommhold, Phys. Rev. A **34**, 2936 (1986).
[2] R. J. Hinde, D. T. Anderson, S. Tam, and M. E. Fajardo, Chem. Phys. Lett. **356**, 355 (2002).
[3] R. J. Hinde, J. Chem. Phys. **119**, 6 (2003).
[4] A. R. W. McKellar, J. Chem. Phys. **105**, 2628 (1996).
[5] L. Frommhold and W. Meyer, Phys. Rev. A **35**, 632 (1987).
[6] C. Bissonnette, K. G. Crowell, R. J. Le Roy, R. J. Wheatley, and W. J. Meath, J. Chem. Phys. **105**, 2639 (1996).
[7] M. J. Frisch, G. W. Trucks, H. B. Schlegel *et al.*, GAUSSIAN 03, Revision B.05, Gaussian, Inc., Pittsburgh, PA, 2003.
[8] J. Čížek, J. Chem. Phys. **45**, 4256 (1966).
[9] G. D. Purvis and R. J. Bartlett, J. Chem. Phys. **76**, 1910 (1982).
[10] J. A. Pople, M. Head-Gordon, and K. Raghavachari, J. Chem. Phys. **87**, 5968 (1987).
[11] S. F. Boys and F. Bernardi, Mol. Phys. **19**, 553 (1979).
[12] D. E. Woon and T. H. Dunning, Jr., J. Chem. Phys. **98**, 1358 (1993).
[13] T. H. Dunning, Jr., J. Chem. Phys. **90**, 1007 (1989).
[14] A. Dalgarno and A. E. Kingston, Proc. R. Soc. London, Ser. A **259**, 424 (1960).
[15] W. Kołos and L. Wolniewicz, J. Chem. Phys. **43**, 2429 (1965).
[16] W. Kołos and L. Wolniewicz, J. Chem. Phys. **46**, 1426 (1967).
[17] F.-M. Tao and Y. K. Pan, J. Chem. Phys. **97**, 4989 (1992).
[18] M. Gutowski, J. Verbeek, J. H. Van Lenthe, and G. Chałasiński, J. Chem. Phys. **111**, 271 (1987).
[19] F.-M. Tao, Int. Rev. Phys. Chem. **20**, 617 (2001).
[20] D. E. Woon, K. A. Peterson, and T. H. Dunning, Jr., J. Chem. Phys. **109**, 2233 (1998).
[21] T. Helgaker, H. J. Aa. Jensen, P. Jørgensen *et al.*, DALTON, Release 1.2 (2001).
[22] W. Meyer and L. Frommhold, Phys. Rev. A **34**, 2771 (1986).
[23] See EPAPS Document No. E-JCPSA6-124-302609 for text files containing the *ab initio* dipole moments for Ar–H_2 and the expansion coefficients $A_{\lambda,L}$ defined in Eq. (4). A direct link to this document may be found in the online article's HTML reference section. This document can be reached via a direct link in the online article's HTML reference section or via the EPAPS homepage (http://www.aip.org/pubservs/epaps.html).
[24] P. Dore, A. Filabozzi, and G. Birnbaum, Can. J. Phys. **66**, 803 (1988).
[25] P. Dore, A. Filabozzi, and G. Birnbaum, Can. J. Phys. **67**, 599 (1989).
[26] F. Mrugała and R. Moszynski, J. Chem. Phys. **109**, 10823 (1998).
[27] J. D. Poll and J. van Kranendonk, Can. J. Phys. **39**, 189 (1961).
[28] J. W. Cooley, Math. Comput. **15**, 363 (1961).
[29] J. L. Hunt, J. D. Poll, and L. Wolniewicz, Can. J. Phys. **62**, 1719 (1984).
[30] J. E. Bohr and K. L. C. Hunt, J. Chem. Phys. **86**, 5441 (1987).
[31] P. W. Fowler and E. Steiner, Mol. Phys. **70**, 377 (1990).
[32] U. Buontempo, S. Cunsolo, and P. Dore, J. Chem. Phys. **62**, 4062 (1975).